Research Article | Vol. 36, No. 8 / August 2019 / Journal of the Optical Society of America A 1361

Journal of the Optical Society of America A
OPTICS, IMAGE SCIENCE, AND VISION

Electrical bandwidth testing of an AOTF transducer as a function of the optical diffraction efficiency

JURGEN VANHAMEL,[1,*] EMMANUEL DEKEMPER,[1] VITALY BORISOVICH VOLOSHINOV,[2] EDDY NEEFS,[1] AND DIDIER FUSSEN[1]

[1]Royal Belgian Institute for Space Aeronomy, Ringlaan 3, 1180 Brussels, Belgium
[2]Physics Faculty, Lomonosov Moscow State University, 119991 Moscow, Russia
*Corresponding author: jurgen.vanhamel@aeronomie.be

Received 29 March 2019; revised 16 June 2019; accepted 1 July 2019; posted 2 July 2019 (Doc. ID 363801); published 18 July 2019

The performance of an acousto-optical tunable filter (AOTF) depends on several key parameters, such as the diffraction efficiency and the applied RF signal at the external network of the transducer. The latter has a specific bandwidth in which its efficiency is high. The goal of this paper is to experimentally investigate the relationship between the electrically matched RF bandwidth and the achieved diffraction efficiency, especially at the edges of the RF frequency band. The experiment revealed that the impedance matching is not completely correlated to the diffraction efficiency. Temperature measurements on the AOTF under test show that, at one edge of the tuning range, the RF signal is converted into a noninteracting acoustic mode.

https://doi.org/10.1364/JOSAA.36.001361

1. INTRODUCTION

The use of acousto-optical tunable filters (AOTFs) is widespread. Several applications exist in which this optical device is used as a filter to detect optical wavelengths at a high temporal and spatial resolution [1]. One of the possibilities is applying an AOTF in a spectrometer [2], but also other applications are feasible, such as space-based imaging systems, using an AOTF in different spectral ranges [3,4]. Understanding the practical maximum range of these devices is important to estimate their applicability.

The working principle of an AOTF is based on the interaction between sound and light inside a birefringent optical cell, in which the Bragg matching condition is valid [5], to select the first-order diffracted light beam at the output (Fig. 1). The sound inside the optical device is generated by means of a transducer, consisting of a piezoelectric layer, responsible for the generation of mechanical vibrations and, consequently, sound waves. This piezoelectric layer is activated by the use of an RF chain, consisting of an RF generator, mutually coupled to an RF amplifier and the AOTF (Fig. 2). To have an efficient conversion of RF energy into sound, the transducer needs to be doubly matched: mechanical impedance matching on the optical cell on one hand, and electrical impedance matching on the RF side on the other hand.

The electrical bandwidth of the transducer is generally used to estimate the optical bandwidth of the AOTF, but in practice, the latter is narrower than expected. The idea of this experiment is to (1) investigate the transducer from an electrical point of view by measuring the voltage standing wave ratio (VSWR) and calculate the bandwidth in which the device is optimally matched from an electrical point of view, (2) investigate the diffraction efficiency (DE) of the optical cell, and (3) compare both results to see if the transducer, especially at the edges of the RF tuning curve, is still capable of generating sound waves. To investigate if applied power is not only transferred into sound, but also into heat, temperature monitoring of the optical cell is done as well.

2. THEORETICAL BACKGROUND

The AOTF analyzed in this work fulfills the so-called parallel tangent condition [6]: a particular acousto-optic interaction geometry in which the momentum-matching condition is more loosely constrained by the angle between the incident light and the acoustic wave phase velocity than in other designs. This tolerance enables a significant acceptance angle, typical of noncollinear devices and attractive for any imaging application. This geometry is illustrated by Fig. 3, where the momentum vectors $\boldsymbol{k_i}$, $\boldsymbol{k_d}$, and $\boldsymbol{K}$ correspond to the incident light, the diffracted light, and the acoustic wave phase velocity, respectively. In the configuration depicted in Fig. 3, the incident light is extraordinary polarized. As a consequence, only 1 order of diffraction is generated (the diffracted beam).

Solving the momentum vector-matching problem yields the relationship between the diffracted optical wavelength and the

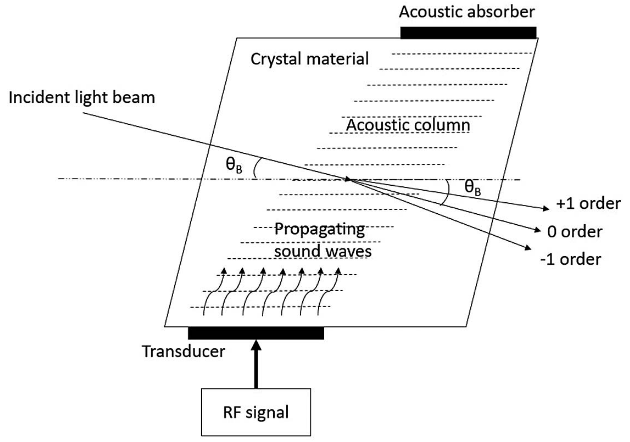

Fig. 1. AOTF concept.

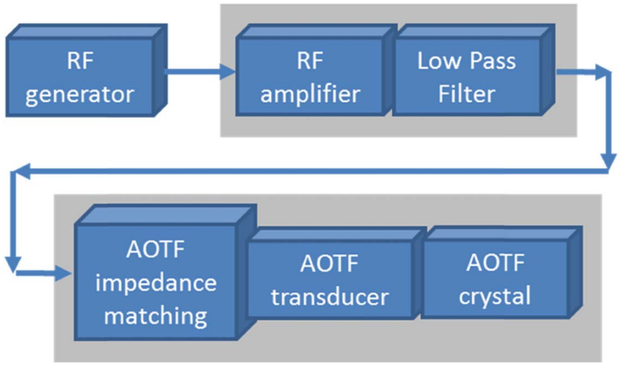

Fig. 2. RF chain concept.

acoustic frequency. This relationship is called the tuning curve of the AOTF, and an approximate expression is

$$f \cong \frac{\Delta n V \sin^2(\theta_i + \alpha)}{\lambda \sin \theta_i}, \tag{1}$$

where f is the acoustic frequency, λ the optical wavelength, $\Delta n = |n_e - n_o|$, θ_i the Bragg angle, V the velocity of the

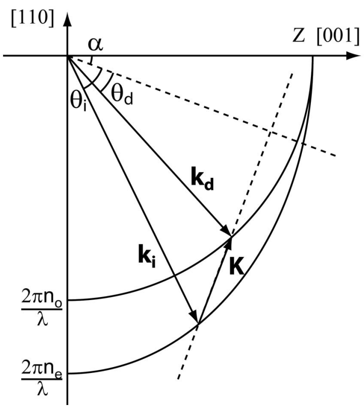

Fig. 3. Wave vector diagram for the acousto-optic interaction in the studied TeO_2 AOTF (reproduced from [3]).

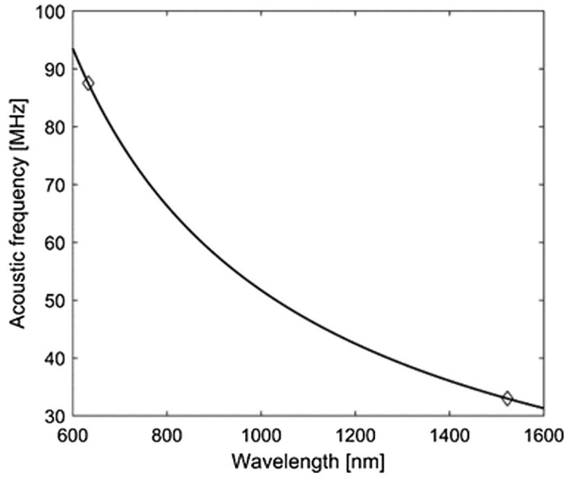

Fig. 4. Tuning curve of the AOTF used in this experiment (parallel tangent configuration). The two diamonds indicate the laser lines that have been used for the experiments carried out in this study.

acoustic wave, and α is the acoustic wave propagation angle with respect to the [110] axis [7]. Figure 4 shows the tuning curve between 600 and 1600 nm when the light incidence angle is chosen such that the parallel tangent condition is fulfilled.

The efficiency of the acousto-optic interaction is generally measured by the DE, i.e., the relative amount of incident photons eligible to Bragg diffraction, which is actually diffracted over the length of the acousto-optic interaction. The easiest way to measure it is by using a laser and to compute Eq. (2), in which I_1 is the intensity of the diffracted beam and I_0 is the incident one,

$$\mathrm{DE} = \frac{I_1}{I_0 + I_1}. \tag{2}$$

Theoretically, the DE is approximated by

$$\mathrm{DE} \cong \sin^2\sqrt{\frac{\pi^2 M_2 L P}{2H\lambda^2}}, \tag{3}$$

in which H is the height, L is the length of the transducer, λ is the optical wavelength, P is the applied acoustic power, and M_2 is the figure of merit [1]. The latter depends on the used material of the acousto-optic device and is calculated as

$$M_2 = \frac{n_i^3 n_d^3 p^2}{\rho V^3}, \tag{4}$$

in which n_i is the refractive index of the incident light, n_d the refractive index of the diffracted light, ρ the mass density of the used crystal, V the velocity of the acoustic wave inside the crystal, and p the photoelastic coefficient. The optimal RF power level for maximum DE can be calculated as follows:

$$P_{\mathrm{sat}} \cong \frac{\lambda^2 H}{2LM_2}. \tag{5}$$

This RF power is applied, via an external impedance network, to the transducer. The transducer can be electrically represented by an $RLC - C_0$ network, known as the Butterworth–Van Dyke (BVD) model [1]. The RF power applied to the transducer has to be converted into sound in the most efficient way.

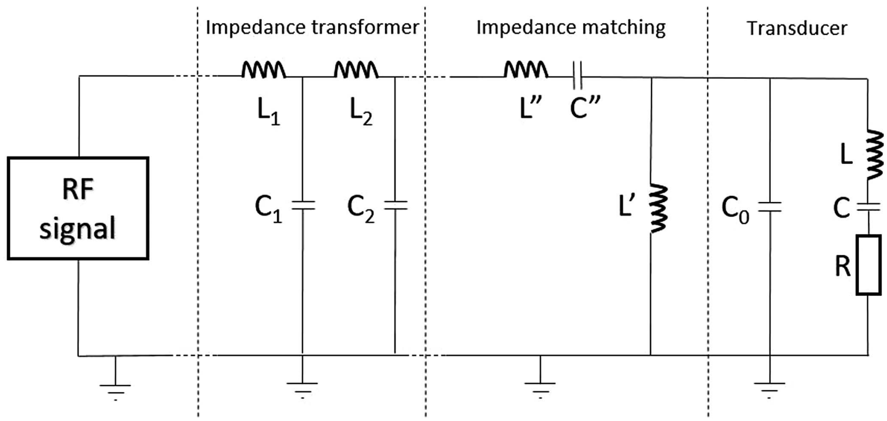

Fig. 5. Transducer setup, external impedance-matching network, and transformer.

To ensure the transducer is seen as mainly a resistive network by the RF chain, an external impedance-matching network is connected to the device (Fig. 5).

The way this network is built and integrated into the AOTF housing depends on the fabrication process. A possible approach to calculate the electrical components of this four-port matching network is based on the theory of Youla [8], Chen and Satyanarayana [9], Zha and Chen [10], and Belikov *et al.* [11] for a third-order Butterworth approach. This consists of an inductor (L') shunted across C_0, combined with a series $L''C''$-network. Based on the coefficients of the third-order Butterworth polynomial (α_{m3}) and the values of the components R, L, C, and C_0, this theory allows us to calculate the maximum bandwidth (BW) of the transducer in which the electrical matching of the device is done in a proper way:

$$BW = 2\pi f \frac{R}{\alpha_{13}}\sqrt{\frac{C}{L}} + 2\pi f \sqrt{\frac{c}{c_0}|x_3| - \frac{R^2 C}{L}(1 - \alpha_{13}^{-2})}. \quad (6)$$

In this formula, f represents the fundamental resonant frequency of the RLC-C_0 network and

$$x_3 = \frac{3\alpha_{33}}{\alpha_{13}} - \alpha_{23}, \quad (7)$$

in which α_{mn} represents the mth coefficient of the n-order Butterworth filter polynomial.

Once this four-port network is built, the impedance at the input of this network is purely resistive. The values of this network, in case of a TeO_2 optical cell, combined with a $LiNbO_3$ piezoelectric transducer, are in the range of a few ohms [9]. In case an RF chain with an output impedance of 50 Ohm is used, a direct connection to the four-port network, although resistive, is not desirable. An additional external network of inductor (L) and capacitor (C) combinations, called the impedance transformer (Fig. 5) and based on the Chebyshev approach, is mandatory [12]. Practically, these LC combinations are limited to a set of two to four, due to the imposed parasitic capacitance.

3. EXPERIMENTAL APPROACH

The first part of the experiment, referred to as the electrical part, consists of measuring the maximum possible RF bandwidth by comparing the forward-standing wave generated towards the transducer, to the reflected wave coming back from the transducer. This comparison leads to the electrical VSWR parameter. The latter is additionally transformed into a power transfer curve ($P/P0$). The higher this value, the more efficient the electrical impedance matching at the transducer performs.

The second part of the experiment is the optical measurement of the DE. The goal is to compare the optical spectrum bandwidth to the electrical one. It is expected that at the edges of the RF bandwidth, the power transfer ratio is high, but the DE is low. If so, electrical matching is still valid, but the mechanical matching is not. In order to drive the AOTF at the edges of its transducer electrical bandwidth, the AOTF has to be used in the deflector configuration. As shown in Fig. 6, it allows us to rely on only two laser lines to explore the entire electrical bandwidth of the transducer [13], when the incident angle is set close to 4–5 deg. The angle between the light incident direction and the [001] axis is equal to $\theta_i + \alpha \approx 12°$.

Based on the curves of Fig. 6, one can see that by working in the region of small Bragg angles (around 4 deg), a single laser wavelength allows us to explore acousto-optic diffraction over a

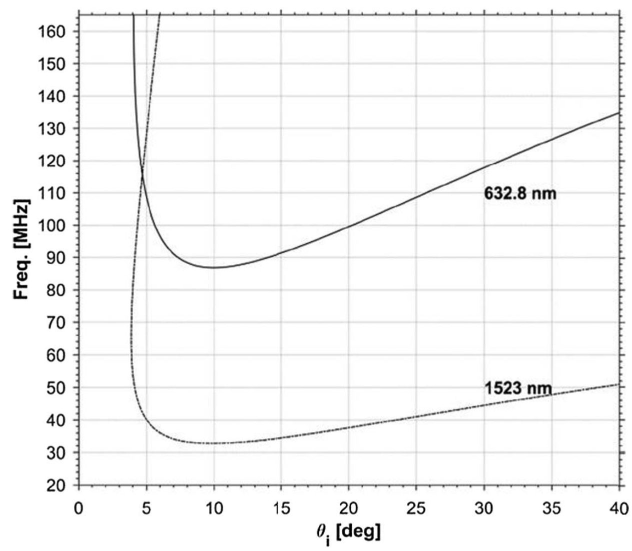

Fig. 6. RF frequency as a function of Bragg angle for the AOTF under test in case of the extraordinary polarized light.

broad acoustic frequency range with minor active readjustment of the position of the AOTF. For each applied electrical frequency, the incidence angle was checked and, if necessary, optimized with respect to DE. In this case, optical beams propagate approximately along one and the same direction in the crystal. Moreover, the optical beams intersect the acoustic column in one and the same place situated at approximately fixed distance from the transducer.

For the investigation of the upper RF frequency range (from 115 to 165 MHz) of the transducer, the 632.8 nm wavelength is used, while for the lower edge (from 57 to 75 MHz), the 1523 nm wavelength is applicable.

4. EXPERIMENTAL SETUP

The used AOTF for this experiment is a device of Gooch and Housego [3] made of TeO_2, and a cut-angle of about 7.6 deg. The applicable RF bandwidth at the transducer is 60–150 MHz based on the information of Gooch and Housego. The authors want to stress that the buildup of the external matching network is unknown. Nevertheless, testing the performance of the external matching network is possible by measuring the VSWR, and transferring this to the power transfer ratio.

The experimental setup (Fig. 7) consists of a 632.8 and 1523 nm laser, a polarizer, the AOTF, and two photodiodes. The latter detect the intensity level of the first- and zero-order light beams. For the 632.8 nm laser, the Thorlabs PM320E energy meter is combined with two SV120 photodiodes. For the 1523 nm laser, a Keithley 6512 electrometer and two Newport 71653 photodiodes are used. The measured intensities yield the DE, based on Eq. (2). The applied laser beam is kept at a physical constant position related to the aperture of the crystal. The AOTF is mounted on a rotation stage to allow for adjustment of the Bragg angle.

The activation of the piezoelectric transducer is done by applying an RF signal at a certain frequency and power. As an RF generator, the R&S SMT-03 is used, mutually connected to the TVA-82-213A+ amplifier of Mini-Circuits. The RF power level is kept at 500 mW for the complete frequency range. This is the power at the input of the electrical network in front of the transducer. A calibration sequence was carried out to make sure the output power is kept constant at the input of the electrical network, taking into account the attenuation and deviation due to the used lab material.

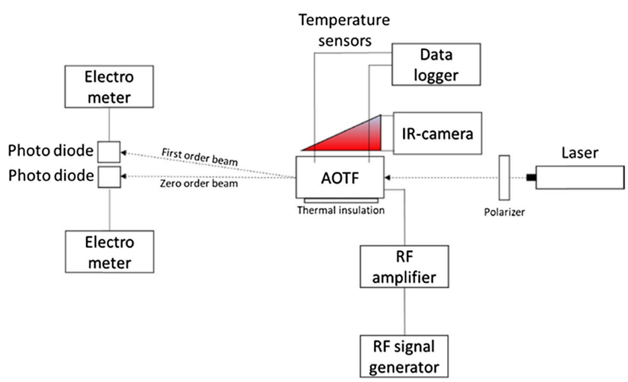

Fig. 7. Optical and RF chain setup.

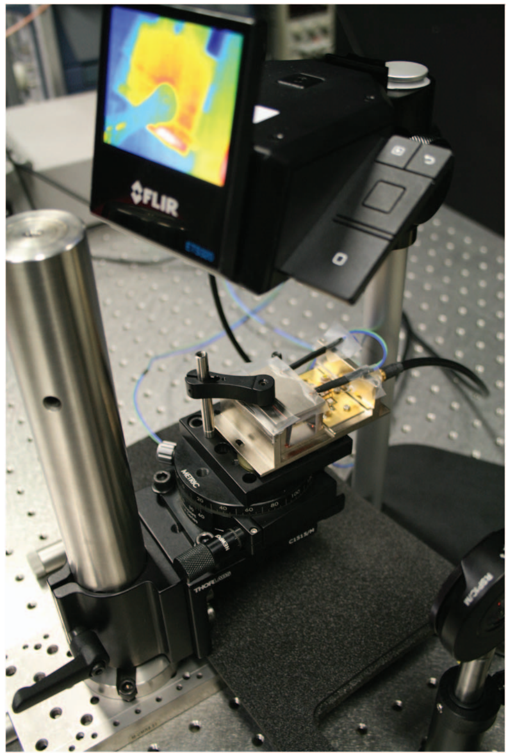

Fig. 8. Position of temperature probes and IR camera.

Because temperature monitoring can give an insight into the conversion of RF energy into heat instead of into sound, two temperature probes are mounted on top of the optical cell. An extra probe is used to monitor the room temperature. All probes are connected to a data logger (HP 34970A). Additionally, a high-sensitivity infrared (IR) camera (FLIR ETS320) is placed above the AOTF to monitor the temperature distribution more closely and from a redundant point of view. Due to the mechanical encapsulation of the crystal, the IR camera monitors the heat distribution on this metal enclosure. The purpose of this additional measurement equipment is to check, by imaging, if any excessive temperature increase can be seen on the housing. By this, the location of the temperature probes can be selected in a proper way. Especially on the edges of the RF bandwidth, the monitoring of the temperature is important. To make sure the heat is not drained into the metal support holding the AOTF, a thermal insulation layer (PEI 1000, polyetherimide) having a low thermal conductivity coefficient, is placed between the AOTF and the metal socket (Fig. 8).

5. EXPERIMENTAL RESULTS

First the VSWR of the transducer is measured and transformed to the power transfer ratio curve (Fig. 9).

Additionally, measurements are carried out by applying an RF frequency starting at 57 MHz, in steps of 1 MHz, up to 75 MHz by using the 1523 nm laser. Each time, the DE is calculated [Eq. (2)] based on the intensity measurements of the zero- and first-order beam. Subsequently, the same measurements are carried out by using the 632.8 nm laser for the upper frequency range of the transducer (115–165 MHz).

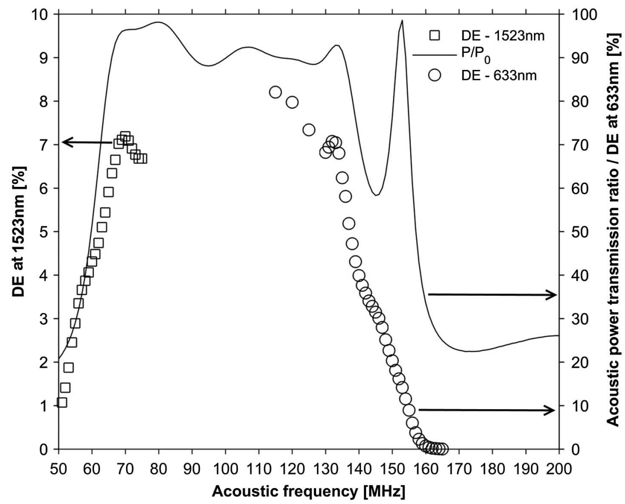

Fig. 9. Combined power transfer ratio curve and DE.

A combined graph (Fig. 9) is made, showing on one hand the power transfer curve of the transducer (full curve) and on the other hand the DE of the AOTF as a function of the frequency (dotted curves).

As can be seen in Fig. 9, the DE obtained with the 1523 nm laser is quite low (less than 10%). This is due to the fact that the RF chain was fully calibrated for a forward RF power of 500 mW, an almost optimal value for the 633 nm light, but not for longer wavelengths, which require more acoustic power, as can be seen from Eq. (5).

Figure 9 indicates that the DE decreases faster at the edges of the tuning range, compared to the power transfer ratio curve. Especially at the upper edge of the frequency range, this effect is clear. This means that the electrical matching is broader than the optical matching of the transducer. The layers between the piezoelectric element and the acoustic cell match less compared to the electrical impedance matching by the external circuit.

In an attempt to identify where the RF energy goes, the temperature variation of the AOTF was monitored by using three probes and an IR camera. Two temperature probes were mounted on top of the AOTF (above the crystal), and a third one was monitoring the room temperature. The experiment consisted in observing the change of the temperature of the device for different signal frequencies (Fig. 10).

We first applied a 90 MHz signal, which corresponds to a nominal working point of the AOTF: good DE and a good power transfer ratio. The temperature of the crystal rose by almost 2 deg compared to the room temperature. After an hour, we switched to 57 MHz, where low DE and poor impedance matching have been observed. The crystal temperature dropped by a few hundreds of mK, indicating that less acoustic energy is present in the crystal. After that, we switched back to 90 MHz and observed a re-increase of the temperature. After stabilization, we switched to 160 MHz and observed a big drop in temperature, in line with the bad impedance matching, although the drop is larger than for 57 MHz, which shows a similar $P/P0$ value. Finally, we switched to 153 MHz, the frequency corresponding to the isolated peak in impedance matching, but where poor DE was observed. Surprisingly, the crystal

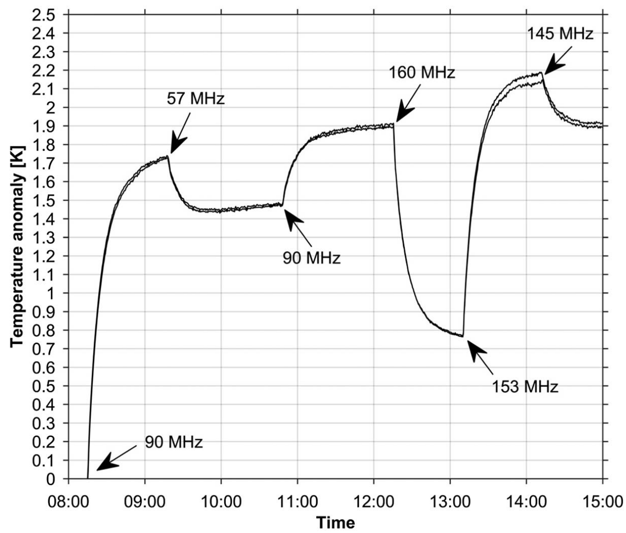

Fig. 10. Temperature anomaly (with respect to room temperature) of the AOTF as a function of time. Annotations show when the electrical signal was changed from a frequency to another. The two temperature probes give almost identical results.

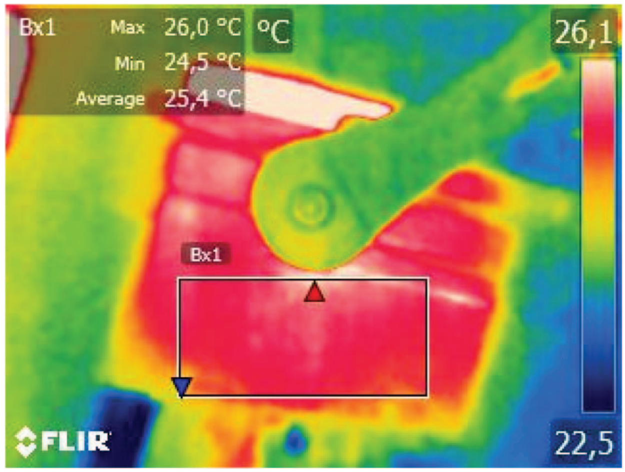

Fig. 11. Temperature variation at the upper edge of the RF frequency band at 160 MHz using the IR camera.

temperature jumped to its highest value, indicating that a significant amount of acoustic energy was present in the crystal. The temperature in Fig. 10 shows a small variation over time. This is due to the slow heating of the complete AOTF package over time. The TeO_2 crystal itself is encapsulated into a small metal cage, which impedes the heat to diffuse easily and causes an equal spreading of the heat. This can be a reason why the variation in temperature is limited. An image of the IR camera measuring 160 MHz is shown in Fig. 11.

6. CONCLUSION

We have tested a commercial TeO_2 AOTF in order to verify the correlation between efficient electrical impedance matching and the optical DE. Our results show that this correlation can fail at the boundaries of the impedance-matching range, indicating that the DE can become small while the impedance matching remains acceptable.

We investigated the relationship between the applied frequency and the heating of the AOTF crystal. We could observe that, in general, a good impedance matching (a good conversion of electrical energy to sound) yields an increase of temperature of the crystal, likely caused by acoustic wave propagation losses. On the contrary, a poor impedance matching obviously yields less acoustic energy in the crystal, and hence a lower crystal temperature.

A notable feature of the AOTF under testing is a peak in impedance matching that does not correspond to a peak in DE. The temperature experiment allowed us to confirm that for this frequency, the transducer is indeed converting a large part of the electrical energy into sound. The fact that this does not correspond to a peak in DE is puzzling. Our main hypothesis is that for this frequency, the transducer vibrates in a regime which not only creates the nominal slow shear wave enabling the acousto-optic interaction, but also another mode of unknown type.

The acoustic beam inside the crystal is absolutely not uniform. Consequently, even if the incidence angle is not changed and the position of the laser beam is kept constant, variations of the frequency result in changes of the acoustic power. This is equivalent to changes in local distribution of power over the volume of the acoustic column.

In general, the experiment carried out confirms that a significant mismatch is possible between the bandwidth of the transducer (defined by the range of good electrical impedance matching) and the bandwidth of the AOTF (defined by the domain of good DE). Users are advised to carry out a similar experiment in order to define the latter.

Funding. PRODEX (4000110400).

Acknowledgment. The authors would like to thank the engineering and solar radiation department at the Royal Belgian Institute for Space Aeronomy, as well as the Faculty of Physics of the Lomonosov Moscow State University for their performed work.

REFERENCES

1. J. Xu and R. Stroud, *Acousto-Optic Devices: Principles, Design and Applications*, Wiley Series in Pure and Applied Optics (Wiley, 1992).
2. E. Dekemper, J. Vanhamel, B. Van Opstal, and D. Fussen, "The AOTF-based NO_2 camera," Atmos. Meas. Tech. **9**, 6025–6034 (2016).
3. E. Dekemper, N. Loodts, B. Van Opstal, J. Maes, F. Vanhellemont, N. Mateshvili, G. Franssens, D. Pieroux, C. Bingen, C. Robert, L. Devos, L. Aballea, and D. Fussen, "Tunable acousto-optic spectral imager for atmospheric composition measurements in the visible spectral domain," Appl. Opt. **51**, 6259–6267 (2012).
4. E. Dekemper, D. Fussen, B. Van Opstal, J. Vanhamel, D. Pieroux, F. Vanhellemont, N. Mateshvili, G. Franssens, V. Voloshinov, C. Janssen, and H. Elandaloussi, "ALTIUS: a spaceborne AOTF-based UV-VIS-NIR hyperspectral imager for atmospheric remote sensing," Proc. SPIE **9241**, 92410L (2014).
5. T. Yano and A. Watanabe, "Acoustooptic TeO_2 tunable filter using far-off-axis anisotropic Bragg diffraction," Appl. Opt. **15**, 2250–2258 (1976).
6. I. C. Chang, "Noncollinear acousto-optic filter with large angular aperture," Appl. Phys. Lett. **25**, 370–372 (1974).
7. N. Gupta and V. B. Voloshinov, "Development and characterization of two-transducer imaging acousto-optic tunable filters with extended tuning range," Appl. Opt. **46**, 1081–1088 (2007).
8. D. Youla, "A new theory of broad-band matching," IEEE Trans. Circuit Theory **11**, 30–50 (1964).
9. W. K. Chen and C. Satyanarayana, "General theory of broadband matching," IEEE Proc. G **29**, 96–102 (1982).
10. Q. Z. Zha and W. K. Chen, "Broad-band impedance matching of the RLC generator and load," J. Franklin Inst. **328**, 317–337 (1991).
11. I. B. Belikov, V. B. Voloshinov, A. B. Kas'yanov, and V. N. Parygin, "Broadband matching of an acouscto-optical-cell transducer using Youla's complex normalization theory," Radioelektronica **31**, 30–35 (1988).
12. G. L. Mattei, "Tables of Chebyshev impedance-transforming networks of low-pass filter form," Proc. IEEE **52**, 939–963 (1964).
13. E. Dekemper, "Development of an AOTF-based hyperspectral imager for atmospheric remote sensing," Ph.D. thesis (Université Catholique de Louvain, 2014), p. 112.